



A Micromechanical Damage Model for Quasi-Brittle Rocks Subjected to Fatigue-Creep Loading

Jin Zhang¹ · Ke Ren¹ · Wen Wang¹ · Wanqing Shen² · Tao Ni³ 

Received: 6 December 2022 / Accepted: 19 February 2023 / Published online: 7 March 2023
© The Author(s), under exclusive licence to Springer-Verlag GmbH Austria, part of Springer Nature 2023

Abstract

To accurately describe the long-term deformation of quasi-brittle rocks, a micromechanical elastoplastic model is proposed for modeling the mechanical responses under cyclic-creep loading. Based on experimental observation, the formation and propagation of microcracks are quantitatively estimated by introducing a micromechanic-based damage variable, which is related to the number of loading cycles and hold time. Thus, the macroscopic property deterioration of material is resulted from the progressive microstructural degradation, which is described by a convolutional law. Different from previous models, the evolution of damage is driven by the deviation from a self-equilibrium state. Within the elastoplastic framework, the fatigue-creep damage evolution is coupled with the plastic deformation, leading to a unified model for both instantaneous and fatigue-creep behaviors of brittle rocks. With the use of a modified returning mapping procedure, the established model is validated by comparing to the experimental results of salt rocks under both constant upper limit cyclic-creep loads and multilevel conditions. Main features of cumulative deformation, fracture mechanism and damage evolution are well captured by the proposed model.

Highlights

- A novel micromechanical model is developed to describe the mechanical behavior of quasi-brittle materials subjected to cyclic-creep loading.
- The fatigue-creep damage is physically related to the progressive microstructural degradation, due to the initiation and propagation of microcracks.
- A convolutional formulation is applied to describe the damage evolution considering the loading cycles and time.
- Numerical simulations are performed and compared to experimental data under both constant upper limit cyclic-creep loads and multilevel conditions.
- The acceleration of fatigue cumulative deformation and damage due to additional creep effects are confirmed.

Keywords Quasi-brittle rocks · Micromechanical · Fatigue-creep effect · Elastoplastic damage model

✉ Tao Ni
nitao_sklgp@cdut.edu.cn

Jin Zhang
chelseazhangjin@163.com

Ke Ren
keren98pl@163.com

Wen Wang
hhdxxw@hhu.edu.cn

Wanqing Shen
wanqing.Shen@polytech-lille.fr

¹ Key Laboratory of Ministry of Education for Geomechanics and Embankment Engineering, Hohai University, Xikang 1, Nanjing 210098, Jiangsu, China

² Department of Civil Engineering, Polytech Lille, UMR 9013-LaMcube, Lille, France

³ State Key Laboratory of Geohazard Prevention and Geoenvironment Protection, Chengdu University of Technology, No. 1 East Third Road, Erxianqiao, Chengdu 610059, Sichuan, China

1 Introduction

In many rock engineering applications, such as underground tunnel supports, seismic activities and blasting excavations, cyclic stresses are regularly encountered. To more accurately assess the long-term stability of rock engineering, it is essential to characterize the deformation and failure mechanism as well as the constitutive model of rocks that are subject to cyclic stresses (Liu and Dai 2021). By experimental observations on the rock materials subjected cyclic loads, the reduction of mechanical properties and different responses have been systematically investigated by researchers based on the loading path (Jia et al. 2018; Kumar et al. 2018), frequency (He et al. 2019), loading type (Vaneghi et al. 2018; Ma et al. 2013), environmental conditions (Jiang and Niu 2016; Sun and Zhang 2019) and other factors.

To evaluate the degradation of material due to fatigue effects, the failure characteristics and fatigue damage have also been analyzed and quantified in available studies by various measurement methods. By generating the fracture bands of damaged rock samples, the fragmentation degree is related to the cyclic loading parameters in Ghamgosar et al. (2017) and Yang et al. (2017). Based on the X-ray micro computed tomography (CT) observations (Yang et al. 2015), rock specimens subjected to cyclic loads contain more complex crack flats than those subjected to monotonic load. Similarly, both the crack region and aperture range in fatigue-damaged rocks exceed those in monotonically failed ones. On the other hand, acoustic emission (AE) technology has also been successfully applied to detect the damage development of tested samples during loading process (Moradian et al. 2016; Jiang et al. 2021). The formation or propagation of microcracks in the defective area will lead to the release of stored energy and recorded AE counts, indicating the internal state of rock. Comparing with the monotonic load, the maximum AE counts get more important with the increase of loading cycles, and the most active AE events occur near the peak stress in each cycle (Zhang et al. 2017; Singh et al. 2018; Tang et al. 2020). Consequently, the degradation of rock material related to the microcracks under cyclic loads is different from that subjected to monotonic load based on the above analysis. And to describe the deformation characteristics due to fatigue effect, the damage state of rock materials related to the microcrack need to be taken into account.

Numerous advancements (Lee and Fenves 1998; Cerfontaine et al. 2017; Zhou et al. 2020) have firstly been produced in the elasto-plastic framework with regard to constitutive modeling of cyclic deformation and failure of rock materials. The fatigue properties are described using the internal state variables (Wang et al. 2013; Liu and Dai 2018). Since energy dissipation frequently occurs along with

the deformation and failure of rocks, constitutive models (Ye and Wang 2001; Liu et al. 2016) from an energy standpoint are built by fusing energy dissipation and damage evolution. Besides, different kinds of empirical laws have also been presented, in particular, by adding the induced damage process, to describe the fatigue damage. A linear-exponential formula, for instance, enhances the inverted-S damage model was proposed by Xiao et al. (2011). In addition, a variety of factors have been considered, including energy dissipation (Miao et al. 2021), loading frequency and rate (Wang et al. 2016; Moreo et al. 2007) and the micro-structure (Sandoval et al. 2020; Baktheer et al. 2021). Recently, an exponential cumulative damage model was presented by He et al. (2019) to predict the lifetime of salt rock based on the discovery of three stages of deformation in fatigue tests.

Within the framework of damage mechanics, important efforts have been concentrated on description of the deterioration of quasi-brittle rocks due to growth and coalescence of microcracks (Dragon and Mroz 1979; Frantziskonis and Desai 1987; Shao et al. 2006; Wu et al. 2006). Considering the distribution of microcracks and microvoids, isotropic and anisotropic damage models have both been formulated with or without the plastic coupling for quasi-brittle materials (Abu-Lebdeh and Voyiadjis 1993; Luccioni and Rougier 2005; Jason et al. 2006), by adopting the micro-plane theory (Carol and Bazant 1997), discrete thermodynamics formulation (Zhu et al. 2010). In particular, in order to make direct use of Eshelby's solution, the microcracks are assumed in penny-shape and the effective elastic tensor are mathematically derived by Zhu et al. (2008) with the isotropic assumption and by applying the Mori-Tanaka (MT) scheme (Mori and Tanaka 1973). This micromechanics-based damage model has been successfully applied to simulate the instantaneous and time-dependent behaviors, volume dilatation and damage-induced softening, and multi-field effects of rock-like materials (Zhu et al. 2016; Zhao et al. 2016; Yuan et al. 2020).

Furthermore, considering the long design service life of rock engineering (usually more than 100 years), the creep effects on the mechanical characteristics and long-term stability can not be ignored. By experimental investigations on the plastic deformation, fatigue life and fracture properties, Zhao et al. (2022b) and Zhao et al. (2022a) have constructed a nonlinear model to describe the damage evolution of salt rock under cyclic loads with constant stress intervals. The acceleration of fatigue deterioration on the material due to creep effects has been also systematically confirmed based on a series of tests (Ma et al. 2021; Wang et al. 2022; Shi et al. 2022). Considering that the accumulated deformation is usually the most essential information needed to be monitored in engineering, the interest is concentrated on the accumulated deformation. And a mathematical function is needed to accurately describe the progressive fatigue-creep induced damage.

With the previous analysis, the present work is devoted to modeling of mechanical responses of quasi-brittle materials subjected to coupled cyclic-creep loading in a concise unified form. Within the elastoplastic damage framework, a fatigue-creep induced damage parameter, related to upper limit stress, loading cycle and hold time, is introduced to describe the degradation of material properties. The homogenization method with assumption of penny-shaped micromcracks is adopted to relate the macroscopic property deduction and the micro-structural degradation. A new evolution law of fatigue-creep damage is proposed by considering the number of cycles and time interval. Different from available models, the evolution of damage is driven by the deviation from a self-equilibrium state (Shao et al. 2003; Pietruszczak et al. 2004). The instantaneous and long-term deformation can be both predicted by the established unified model.

This paper is organized in the following way. In Sect. 2, a micromechanics-based damage parameter is decomposed for cracked body based on the micro-CT observations, and a convolutional formulation is introduced for the description of damage evolution. Then, a unified elastoplastic damage model is formulated by incorporating the fatigue-creep damage in Sect. 3. To access the accuracy of the proposed model, a non-linear explicit integral algorithm based on the returning mapping procedure is developed for the numerical program in Sect. 4. Comparisons between numerical predictions and experimental results are also carried out for both constant upper limit cyclic-creep loads and multilevel conditions. The last section is devoted to the conclusions.

2 Experimental Analysis of Rock Samples under Fatigue-Creep Loading and Micromechanical Formulations of Damage Evolution

In this section, the material degradation is firstly analyzed by experimental observation of rock specimens under coupled cyclic-creep loads. A damage variable decomposed

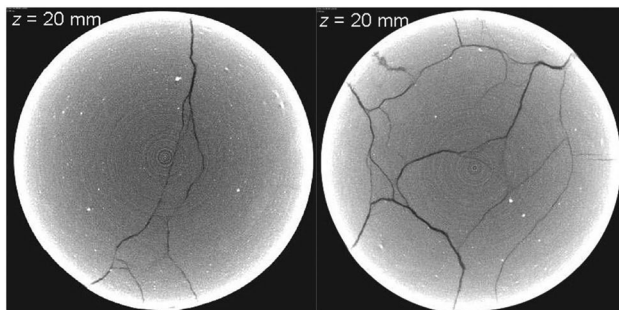


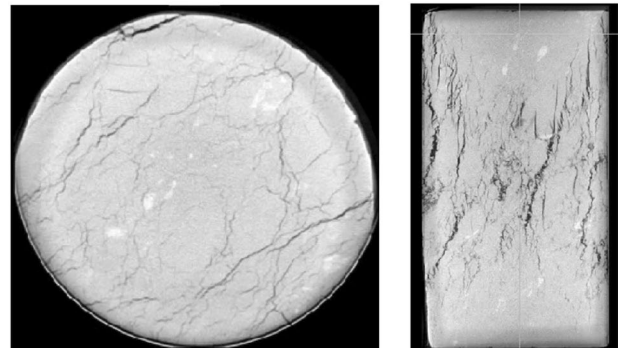
Fig. 1 CT scanning images of rock specimens under monotonic load (left) and cyclic load (right) by Yang et al. (2015)

to fatigue and creep parts is introduced to depict the effective mechanical properties of material. In the framework of micromechanics, a mathematical formulation is then adopted to describe micro-structural evolution.

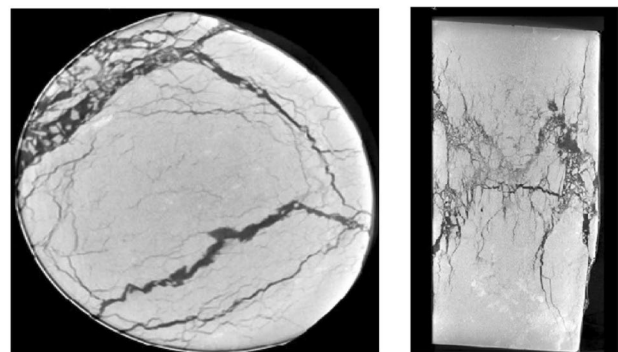
2.1 Experimental Observation of Fatigue-Creep Tests and Damage Decomposition

Firstly, by comparison of micro-CT scanning images, fracture morphology of rock specimens subjected to monotonic and cyclic loads is studied by Yang et al. (2015). As shown in Fig. 1, the ruptured section is featured more complex with micro-cracks under cyclic load than that under monotonic load. Both the crack region and aperture range in cyclically failed specimens surpass those in monotonic way, which is considered as the consequence micro-structural degradation. Consequently, the progressive degradation of cracked body is described by an additional damage variable related to the micro-structure.

Moreover, to reveal the crack pattern of rock material due to fatigue-creep coupling effects, Zhao et al. (2022a) have scanned salt samples experienced cyclic loadings without



(a) Top (left) and front surfaces (right) of the salt samples subjected to cyclic loads with intervals of 0s (without creep effect).



(b) Top (left) and front surfaces (right) of the salt samples subjected to cyclic loads with intervals of 40s (coupled fatigue-creep effect).

Fig. 2 CT images of the salt samples after cyclic tests with constant stress intervals of 0 s **(a)** and 40 s **(b)** by Zhao et al. (2022a)

and with stress intervals to obtain the fracture structure. CT slices extracted from top and front surfaces of salt samples are provided in Fig. 2. Concerning the top surface of tested samples, few main cracks and numerous branch cracks can be observed in Fig. 2a in which the salt sample has experienced cyclic loads without hold time (constant stress intervals of 0 s). Differently, for the salt sample with the hold time per cycle of 40 s (Fig. 2b), many through cracks and pores are characterized on the top surface. The crack width in Fig. 2b presents a marked increase compared to that in which the rock is not subjected to constant stress intervals (Fig. 2a). This is due to the continuously exerted load on the rock sample leading to an additional damage component during the cyclic loading process.

Similarly, according to the CT images from the front view, a main through cracks is also observed with more branched cracks in Fig. 2b. Consequently, the creep effect (constant stress interval) will lead to an additional accumulation to the fatigue damage during load process. Based on the experimental observation, Zhao et al. (2022a) has proposed the damage variable as $\omega = \frac{A-\bar{A}}{A}$ to quantitatively describe deterioration of the cracked material, defining the total area of intact material as A and the real effective area of microcracked section as \bar{A} .

It can be concluded from Figs. 1 and 2 that fatigue and creep effects will both lead to more microcracks on the tested rock samples. So we propose a cracked-related damage parameter, where the fatigue and creep effects should be taken into account. Inspired from the unified model for describing the instantaneous and time-dependent damage by Zhao et al. (2016), the total damage due to nucleation and growth of microcracks can be decomposed into two parts

$$\omega = \omega^c + \omega^f \quad (1)$$

where ω^c and ω^f represent respectively the creep and fatigue damage, leading to the material deterioration.

2.2 Micromechanical-based Formulation for Damage Variable and Effective Mechanical Property of Material

By CT scanning of tested rock samples, additional branch cracks are observed after subjected to cyclic-creep load. To this end, a micromechanical formulation for the description of fatigue-creep induced damage in cracked media is introduced in this subsection, and a linear form defining the damage evolution is provided.

For later use, we consider a representative elementary volume (REV) to represent the idealized micro-structure of the material. The intact material is supposed to be linearly isotropic, and the initial fourth-order elastic tensor takes the following form

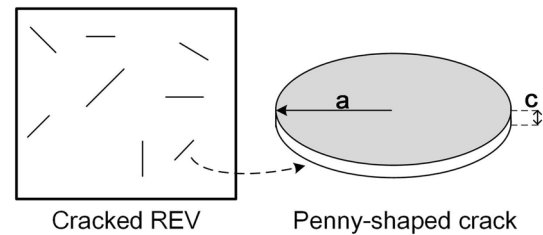


Fig. 3 Cracked representative elementary volume (REV) containing randomly distributed and oriented penny-shaped cracks

$$C_{ijkl}^0 = 3kJ_{ijkl} + 2\mu K_{ijkl} \quad (2)$$

where k and μ are the bulk and shear moduli of undamaged material. Besides, $J_{ijkl} = \frac{1}{3}\delta_{ij}\delta_{kl}$ denotes the fourth-order hydrostatic projector and $K_{ijkl} = \frac{1}{2}(\delta_{ik}\delta_{jl} + \delta_{il}\delta_{jk}) - \frac{1}{3}\delta_{ij}\delta_{kl}$ represents the deviatoric one.

The relevant REV of damaged brittle material is described by a matrix-inclusions system composed of an isotropic matrix and a large number of randomly distributed and oriented microcracks. Inspiring from the micromechanical studies of rock materials (Zhu et al. 2016; Zhao et al. 2016), all microcracks are assumed to be penny-shaped in geometry and characterized by the aspect ratio $\epsilon = c/a \ll 1$ with a and c denoting the average radius and the half opening of cracks, respectively (see Fig. 3). The volume fraction of a family of microcracks can be expressed mathematically as

$$\varphi = \frac{4}{3}\pi a^2 c \mathcal{N} = \frac{4}{3}\pi \epsilon \omega \quad (3)$$

with \mathcal{N} being the number of cracks per unit volume of all microcracks. As a result, the crack density parameter ω , related to the degradation of material, represents the fatigue-creep induced isotropic damage of material, having the following expression:

$$\omega = \mathcal{N}a^3 \quad (4)$$

According to Zhu et al. (2016), the homogenized effective fourth-order elastic tensor of microcracked body can be obtained by applying Mori–Tanaka scheme with isotropic assumption

$$C_{ijkl}(\omega) = \frac{1}{1 + \alpha_1\omega} 3kJ_{ijkl} + \frac{1}{1 + \alpha_2\omega} 2\mu K_{ijkl} \quad (5)$$

where α_1 and α_2 are two damage constants only function of Poisson's ratio ν of intact material. For penny-shaped microcracks, the damage constants α_1 and α_2 can be rigorously derived as

$$\alpha_1 = \frac{16}{9} \frac{1 - \nu^2}{1 - 2\nu}, \quad \alpha_2 = \frac{32}{45} \frac{(1 - \nu)(5 - \nu)}{2 - \nu} \tag{6}$$

To avoid repetition, the derivations are provided in Appendix A.

2.3 Evolution of Fatigue-Creep Induced Material Degradation

It is assumed that two dissipation mechanisms should be taken into account, plastic deformation and damage due to growth of microcracks. To describe the fatigue-creep damage behavior in loading process within the elastoplastic framework, it is also essential to determine the damage evolution law.

In the experimental observations in both cyclic and creep tests (Liu and Dai 2021), three stages of irreversible deformation curves can be distinguished. Consequently, a stationary state potentially exists related to the steady stage. For quantitative description of cycle-dependent and time-dependent damage $\omega(n, t)$, a parameter $\bar{\omega}$ is introduced to describe the internal state of microstructural degradation. Referring to a study devoted to creep deformation (Pietruszczak et al. 2004), the evolution rate is described by the following equilibrium equation:

$$\dot{\omega} = \gamma(\bar{\omega} - \omega) \tag{7}$$

in which $\dot{\omega}$ represents the damage evolution rate and $\bar{\omega}$ denotes the equilibrium state of microstructural degradation. The parameter γ controls the kinetics of damage evolution. It is obvious that when $\omega \leq \bar{\omega}$, there is an increase of microstructural degradation. Its kinetics is driven by the distance between the current state and the equilibrium one ($\bar{\omega} - \omega$). When the current state approaches the stationary one, $\omega \rightarrow \bar{\omega}$, the damage evolution decreases and eventually vanishes.

Since the total damage due to coupled cyclic-creep load is decomposed to two parts (1), the fatigue and creep effects both need to be considered in the formulation of damage variable. Combining with the evolution rate formulation (7), the total damage is recast to the incremental form

$$d\omega = d\omega^f + d\omega^c = \gamma^f(\bar{\omega} - \omega)dn + \gamma^c(\bar{\omega} - \omega)dt \tag{8}$$

where γ^f and γ^c are materials constants controlling the rate of damage due to fatigue and creep, respectively.

Supposing that at the initial state, there is no damage for intact material ($\omega(0) = 0$ and $\omega \in [0, \bar{\omega}]$). By applying the Laplace transform and convolution operation to Eq.(1), the total damage of material after N cycles and t duration can be obtained by the integral function:

$$\omega = \int_0^N \bar{\omega}(n, \tau) \gamma^f e^{-\gamma^f(N-n)} dn + \int_0^t \bar{\omega}(n, \tau) \gamma^c e^{-\gamma^c(t-\tau)} d\tau \tag{9}$$

The exponential terms $e^{-\gamma(N-n)}$ and $e^{-\gamma^c(t-\tau)}$ define the memory functions, allowing considering the dependency of coupled fatigue-creep damage on the number of cycles and hold time. The detailed derivation of the integral form (9) is provided in Pietruszczak et al. (2004) and Shao et al. (2003).

In coupled cyclic-creep loading condition, the accumulation of inelastic strain deformation depends on the number of cycles and time duration. Therefore, the micro-structural damage variable ω , its stationary value $\bar{\omega}$ and evolution rate are all functions of accumulated inelastic strain. In particular, according to the researches on creep damage of rock materials (Shao et al. 2003; Pietruszczak et al. 2004), the determination of stationary damage parameter $\bar{\omega}$ characterizing the self-equilibrated state and microstructural evolution is a key relation to be defined. This issue will be discussed in the next section.

3 Formulation of Fatigue-Creep Damage Model for Quasi-Brittle Materials

In the current section, a novel fatigue-creep damage model is formulated for modeling the mechanical behavior of quasi-brittle materials under coupled cyclic and creep loads by incorporating material degradation of the microcracked body. The introduced fatigue-creep damage will be implemented in the micromechanical elastoplastic framework to predict the deformation under different loading condition with a unified form.

3.1 Basic Elastoplastic Constitutive Relations

The basic mechanical behavior of rocks is assumed to be described by elastoplastic models, and the total local strain is decomposed into elastic and plastic parts

$$\epsilon_{ij} = \epsilon_{ij}^e + \epsilon_{ij}^p \tag{10}$$

So the elastoplastic strain–stress relation is expressed in the general form:

$$\sigma_{ij} = C_{ijkl}(\omega)(\epsilon_{kl} - \epsilon_{kl}^p) \tag{11}$$

where the effective fourth-order elastic stiffness tensor $C_{ijkl}(\omega)$ of damaged material is defined by Eq.(5), and σ_{ij} denotes the Cauchy stress tensor.

Accordingly, considering the degradation of elastic property constants, the constitutive relation (11) can be recast to the following incremental form:

$$d\sigma_{ij} = C_{ijkl}(d\varepsilon_{kl} - d\varepsilon_{kl}^p) + \frac{\partial C_{ijkl}}{\partial \omega} (\varepsilon_{kl} - \varepsilon_{kl}^p) d\omega \quad (12)$$

in which

$$\frac{\partial C_{ijkl}}{\partial \omega} = -\frac{\alpha_1}{(1 + \alpha_1 \omega)^2} 3kJ_{ijkl} - \frac{\alpha_2}{(1 + \alpha_2 \omega)^2} 2\mu K_{ijkl} \quad (13)$$

For the description of plastic strain, a yield function is firstly defined. Since the peak strength will not be reached in cyclic and creep tests, we adopt the following nonlinear plastic yield function and hardening rule, which have been applied to describe the mechanical behaviors of quasi-brittle materials (Chiarelli 2000; Shao et al. 2003) to guarantee the accuracy before the peak strength:

$$f(\sigma_{ij}, \alpha_p) = \sigma_{eq}^2 + A \alpha_p (\sigma_m - C) \leq 0 \quad (14)$$

where σ_m denotes the mean stress, and σ_{eq} is the deviatoric stress, defined as:

$$\sigma_m = \frac{1}{3} \sigma_{kk}, \quad \sigma_{eq} = \sqrt{\frac{3}{2} (\sigma_{ij} - \sigma_m \delta_{ij}) (\sigma_{ij} - \sigma_m \delta_{ij})} \quad (15)$$

The parameters A and C are respectively related to the maximum frictional coefficient and the cohesion of material at the failure state. On the other hand, inspired from the experimental investigation of hard claystone (Chiarelli 2000), an isotropic hardening law is adopted in the following hyperbolic form, where the frictional coefficient activation parameter α_p varies from its initial value α_p^0 to 1:

$$\alpha_p(\gamma^p) = \alpha_p^0 - \left(1 - \alpha_p^0\right) \frac{\gamma^p}{\gamma^p + B} \quad (16)$$

The plastic hardening rate is controlled by the parameter B , and γ^p is the equivalent plastic shear strain and defined by:

$$\gamma^p = \int \sqrt{\frac{2}{3} d\varepsilon_{ij}^p d\varepsilon_{ij}^p}, \quad \varepsilon_{ij}^p = \varepsilon_{ij}^p - \frac{1}{3} \varepsilon_{kk}^p \delta_{ij} \quad (17)$$

Consequently, the proposed fatigue damage model can capture the main mechanical property in monotonic case before peak strength and be expressed in a concise form.

Based on the experimental and theoretical works on geological materials, a non-associated flow rule is usually necessary due to complex plastic deformation kinetics, for instance the transition from volumetric compressibility to dilatancy (Shao et al. 2003; Pietruszczak et al. 1988). As a result, we adopt the same plastic potential function:

$$g(\sigma_{ij}) = \sigma_{eq} + A \eta (\sigma_m - C) \ln (\sigma_m - C) = 0 \quad (18)$$

where the parameter η controls the sign of plastic volumetric strain. Hence, the plastic strain increments are given by the flow rule:

$$d\varepsilon_{ij}^p = d\lambda \frac{\partial g}{\partial \sigma_{ij}} \quad (19)$$

where $d\lambda$ is the non-negative plastic multiplier, which is determined from the plastic consistency condition in the following derivation.

3.2 Formulation of Coupled Fatigue-Creep Damage Model

Based on experimental studies (Fan et al. 2016; Wang et al. 2021), the elastic properties and the failure strength of materials are both weakened by the fatigue-creep induced damage. The basic elastoplastic model in the previous subsection is now extended to cyclic-creep loading by incorporating fatigue-creep damage effects.

With the assumption of penny-shaped microcracks in rock materials due to fatigue and creep effects, the micromechanical-based homogenized elastic properties is defined by the effective fourth-order tensor (5). Accordingly, the effective bulk and shear moduli are

$$k^{\text{eff}}(\omega) = \frac{1}{1 + \alpha_1 \omega} k, \quad \mu^{\text{eff}}(\omega) = \frac{1}{1 + \alpha_2 \omega} \mu \quad (20)$$

Similarly, the maximum frictional coefficient A is assumed in function of the damage variable, taking the linear form:

$$A^{\text{eff}}(\omega) = (1 - \alpha \omega) A \quad (21)$$

in which the micromechanical damage parameters α_1 and α_2 are only in function of Poisson's ratio controlling the degradation rate, and α need to be determined experimentally.

Moreover, the plastic yield function and potential of damaged materials are also extended to the following forms coupling with the fatigue-creep damage:

$$\begin{aligned} f(\sigma_{ij}, \alpha_p, \omega) &= \sigma_{eq}^2 + A^{\text{eff}} \alpha_p (\sigma_m - C) \leq 0 \\ g(\sigma_{ij}, \omega) &= \sigma_{eq} + A^{\text{eff}} \eta (\sigma_m - C) \ln (\sigma_m - C) = 0 \end{aligned} \quad (22)$$

The plastic consistency condition is expressed as follows by considering the material degradation and plastic hardening:

$$df = \frac{\partial f}{\partial \sigma_{ij}} d\sigma_{ij} + \frac{\partial f}{\partial \alpha_p} d\alpha_p + \frac{\partial f}{\partial \omega} d\omega = 0 \quad (23)$$

The increment of coupled fatigue-creep damage is defined by Eq.(8).

3.2.1 Instantaneous Loading Stage

The proposed elastoplastic fatigue damage model is applied to strain-prescribed instantaneous loading

condition in this part. The damage increment is null in this case: $d\omega = 0$.

Substituting the stress–strain relations (12), the plastic hardening law (16) and the plastic flow rule (19) for plastic consistency condition (23), one can derive the plastic multiplier as follows:

$$d\lambda = \frac{\frac{\partial f}{\partial \sigma_{ij}} C_{ijkl} d\epsilon_{kl}}{\frac{\partial f}{\partial \sigma_{pq}} C_{pqrs} \frac{\partial g}{\partial \sigma_{rs}} - \frac{\partial f}{\partial \alpha_p} \frac{\partial \alpha_p}{\partial \gamma^p} \frac{\partial g}{\partial \sigma_{eq}}} \quad (24)$$

Putting the plastic multiplier (24) into the strain–stress relation (12), the general incremental form of the constitutive equations can be obtained for stain-prescribed instantaneous condition:

$$d\sigma_{ij} = C_{ijkl}^{tan} d\epsilon_{kl} \quad (25)$$

where C_{ijkl}^{tan} denotes the fourth-order tangent stiffness tensor, given by:

$$C_{ijkl}^{tan} = C_{ijkl} - \frac{1}{H_\sigma} C_{ijpq} \frac{\partial g}{\partial \sigma_{pq}} \frac{\partial f}{\partial \sigma_{rs}} C_{rskl} \quad (26)$$

It is obvious that for monotonic loading case, the constructed model can reduced to the same one as proposed in Shao et al. (2003) by considering $d\omega = 0$. The material properties are not degraded without fatigue and creep damage.

3.2.2 Stress-Prescribed Coupling Fatigue-Creep Loading

For simulation of fatigue-creep tests, it is convenient to formulate the constitutive model for stress-prescribed loading conditions. For this purpose, the effective fourth-order elastic compliance tensor of damaged rock materials is defined as

$$D_{ijkl} = (C_{ijkl})^{-1} = (1 + \alpha_1 \omega) \frac{1}{3k} J_{ijkl} + (1 + \alpha_2 \omega) \frac{1}{2\mu} K_{ijkl} \quad (27)$$

Then, the total strain tensor can be determined by:

$$\epsilon_{ij} = D_{ijkl} \sigma_{kl} + \epsilon_{ij}^p \quad (28)$$

Accordingly, the increment form of strain tensor takes the following form:

$$d\epsilon_{ij} = D_{ijkl} d\sigma_{kl} + \frac{\partial D_{ijkl}}{\partial \omega} \sigma_{kl} d\omega + d\lambda \frac{\partial g}{\partial \sigma_{ij}} \quad (29)$$

where the differential term reads

$$\frac{\partial D_{ijkl}}{\partial \omega} = \frac{\alpha_1}{3k} J_{ijkl} + \frac{\alpha_2}{2\mu} K_{ijkl} \quad (30)$$

Taking account of the fatigue-creep damage, the plastic consistency condition (23) in stress-prescribed loading condition can be written as

$$\frac{\partial f}{\partial \sigma_{ij}} d\sigma_{ij} + \frac{\partial f}{\partial \alpha_p} \frac{\partial \alpha_p}{\partial \gamma^p} d\gamma^p + \frac{\partial f}{\partial A^{eff}} \frac{\partial A^{eff}}{\partial \omega} d\omega = 0 \quad (31)$$

in which

$$d\gamma^p = d\lambda \frac{\partial g}{\partial \sigma_{eq}}, \quad \frac{\partial A^{eff}}{\partial \omega} = -\alpha A \quad (32)$$

Substituting the above expressions of ((32)) into the plastic consistency condition (31), the plastic multiplier can be obtained

$$d\lambda = \frac{\frac{\partial f}{\partial \sigma_{ij}} d\sigma_{ij} - \alpha A \frac{\partial f}{\partial A} d\omega}{H_\sigma} \quad (33)$$

where the plastic hardening modulus H_σ is given by:

$$H_\sigma = -\frac{\partial f}{\partial \alpha_p} \frac{\partial \alpha_p}{\partial \epsilon_{eq}^p} \frac{\partial g}{\partial \sigma_{eq}} \quad (34)$$

By using the expressions of the plastic multiplier (33) and of the elastic strain increment (29), one has the incremental form of strain–stress relations for elastoplastic damaged materials under stress-prescribed conditions:

$$d\epsilon_{ij} = D_{ijkl}^{tan} d\sigma_{kl} + \Psi_{ij} d\omega \quad (35)$$

D_{ijkl}^{tan} is the fourth-order tangent compliance tensor given by:

$$D_{ijkl}^{tan} = D_{ijkl} + \frac{1}{H_\sigma} \frac{\partial g}{\partial \sigma_{ij}} \frac{\partial f}{\partial \sigma_{kl}} \quad (36)$$

The second-order tensor Ψ_{ij} defines the effect of fatigue-creep damage:

$$\Psi_{ij} = \frac{\partial D_{ijkl}^0}{\partial \omega} \sigma_{kl} - \frac{1}{H_\sigma} \alpha A \frac{\partial f}{\partial A} \frac{\partial g}{\partial \sigma_{ij}} \quad (37)$$

It is noticed that the total strain increment (35) is divided into two terms. The first one provides the strain due to stress variation in elastoplastic damaged materials under monotonic loading. The second term represents the strain variation induced by the evolution of fatigue-creep damage during loading process. Besides, the proposed model can also be applied to predict the cumulative deformation in unique fatigue or creep tests by taking $dt = 0$ or $dn = 0$, respectively.

3.3 Definition the Microstructure Evolution Parameter $\bar{\omega}$

To be implemented in numerical procedure, the microstructure evolution parameter $\bar{\omega}$ need to be defined to describe the degradation of material in cyclic and creep stage. From the acoustic emission observation of entire loading process, the material degradation evolves with the fatigue-creep damage. It is also confirmed that the fatigue and creep deformation of tested samples is directly proportional to AE activity. Consequently, the variation of $\bar{\omega}$ depends on the loading history, in particular closely related to plastic strains. Based on the above analyses, the variation of $\bar{\omega}$ depends on the loading history, in particular plastic strains. Inspired from the time-dependent deformation of brittle rocks (Zhu et al. 2016), it is assumed that $\bar{\omega}$ related to the generalized plastic strain γ^p by the following function:

$$\bar{\omega} = C_1 \alpha_p e^{\frac{\langle \gamma^p - \gamma_c^p \rangle}{\gamma_c^p}} \quad (38)$$

where $\langle a \rangle = \frac{a+|a|}{2}$ is the Macauley bracket to describe the sudden collapse of rock material in cyclic-creep tests. γ_c^p is the critical value of the generalized plastic strain at failure strength. It corresponds to the peak stress in uniaxial compression test. According to Eq.(38), when $\gamma^p = \gamma_c^p$, accelerated stage starts. C_1 is a model parameter.

4 Numerical Applications to Cyclic-Creep Tests

In this section, the established elastoplastic damage model is validated by comparing with available experimental data. First of all, a modified numerical procedure by returning mapping algorithm is provided in the first subsection. Then, the applications to both constant upper limit stress with long hold time and multi-level cyclic loads with stress interval for salt rocks are carried out.

4.1 Numerical Implementation of the Proposed Model

The proposed model is implemented in the numerical procedure though the emphasis is put on the mechanical response of a material point. The whole loading history is divided into a number of steps. Starting from the initial conditions, it is assumed that the values of stresses, strains, generalized plastic strain and fatigue-creep damage are all known at the beginning of each step. An increment of load, cycle number or time is prescribed at each step. The solutions to determine are the corresponding stresses and accumulated strain due

to loading cycles and time interval, by using the proposed constitutive relations.

Different from classical monotonic elastoplastic model, the cycle- and time-dependent damage parameter ω also need to be calculated and updated at each step. The evolution of fatigue damage is here described by the specific integral function (9). Similarly to monotonic loading, the cyclic-creep load process is also divided into a series of increments. For each increment step, a variation of fatigue damage is evaluated according to (7). Considering cyclic load condition with a constant stress interval, the damage increment is coupled in each load cycle, as defined by Eq.(8). Thus, inspired by the study of creep deformation (Zhu et al. 2016) and after a rigorous mathematical transformation, the following non-linear explicit integral algorithm is adopted:

$$\omega_k = \omega_{k-1} e^{-(\gamma^f dn_k + \gamma^c dt_k)} + \left(\frac{\bar{\omega}_k + \bar{\omega}_{k-1}}{2} \right) e^{-\frac{1}{2}(\gamma^f dn_k + \gamma^c dt_k)} (\gamma^f dn_k + \gamma^c dt_k) \quad (39)$$

It is found that the current value of fatigue damage ω_n depends on the values of stationary damage variable at the current and previous steps, say $\bar{\omega}_k$ and $\bar{\omega}_{k-1}$. As mentioned above, the variation of $\bar{\omega}$ depends on the loading history, in particular plastic strains.

It is supposed that the cycle increment $dn_k = 1$ and the time interval between two cycles noted as $T(dt_k)$, the constant part $\gamma^c dt$ in creep-induced damage (39) remains unchanged in a single load cycle. Thus, the computation of total damage can be simplified by an additional relation between $\gamma^c dt$ (creep-induced damage) and $\gamma^f dn$ (fatigue-induced damage). In practice, the damage increment due to creep is calculated within each load cycle with this additional relation, so the time increment dt_k is not needed in the numerical procedure.

The numerical implementation is based on the standard return mapping algorithm. Due to the material non-linearity, an iterative procedure is needed. Each iteration is composed of elastic prediction and plastic-damage correction. The local integration for calculating deformation at k th increment or the cumulative ones at k th cycle is in the following order

1. At the end of $(k-1)$ th loading increment (monotonic phase) or for $(k-1)$ th cycle (cyclic phase)/time increment, σ_{k-1} , ϵ_{k-1} , ϵ_{k-1}^p , $\bar{\omega}_{k-1}$ and ω_{k-1} are known.
2. Given a new stress increment $d\sigma$ or a new loading cycle increment dn (the creep-induced damage increment is computed in each cycle), then the total stress $\sigma_k = \sigma_{k-1} + d\sigma$ and total cycle $n_k = n_{k-1} + dn_k$.
3. If $d\sigma \neq \mathbf{0}$ and $dn = 0$ (or $dt = 0$), go to (4); if $d\sigma = \mathbf{0}$ and $dn \neq 0$ (or $dt \neq 0$), go to (5).

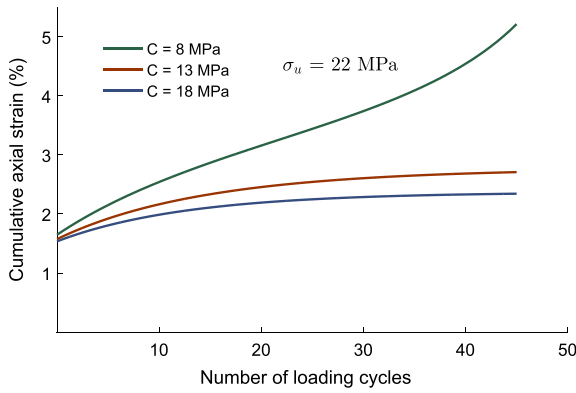


Fig. 4 Parametric analysis on the influence of strength parameter C with constant upper stress $\sigma_u=22$ MPa

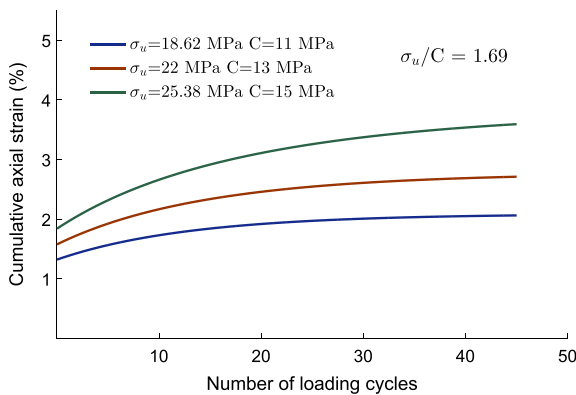


Fig. 5 Parametric analysis on the influence of strength and upper stress with constant stress ratio $\sigma_u/C=1.69$

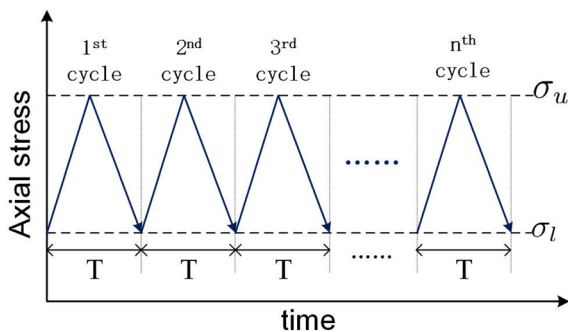


Fig. 6 Schematic diagram of long-period cyclic loading and unloading waveform

4. Check $f(\sigma_k) \leq 0$. If $f(\sigma_k) \leq 0$, $d\epsilon_k^p = \mathbf{0}$ and $\mathbb{D}_k^{tan} = \mathbb{D}^0$; else, calculate the plastic multiplier $d\lambda$ by Eq.(33) and calculate $d\epsilon_k^p$ and \mathbb{D}_k^{tan} by Eq.(36). Then go to (6).

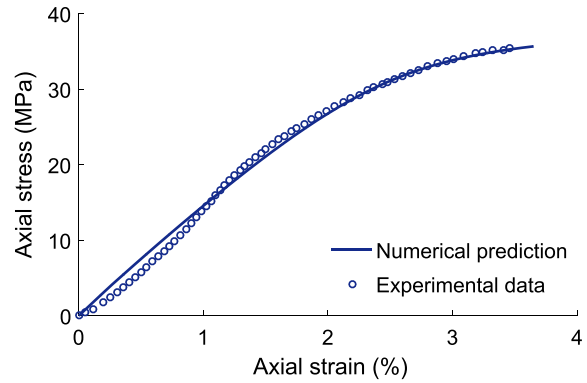


Fig. 7 Comparison between numerical results and experimental data (obtained from Wang et al. 2021) of axial strain in uniaxial compression test on salt rock

5. Calculate $\bar{\omega}_k, \omega_k$ and $\dot{\omega}_k$ by Eq.(38), (39) and (7), respectively. Check $f(\sigma_k) \leq 0$. If $f(\sigma_k) \leq 0$, $d\epsilon_k^p = \mathbf{0}$; else calculate $d\epsilon_k^p$.
6. Update $\bar{\omega}_k$ and ω_k, ϵ_k^p and $\epsilon_k = \mathbb{D}_k^0 : d\sigma + \epsilon_k^p$ or by (35).

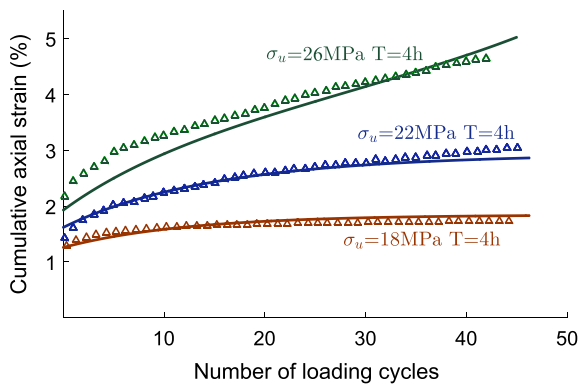
Before carrying out numerical simulation of cyclic tests, we are concerned with the influence of strength parameter of material involved in the final formulation (35) in Fig. 4. It is seen that the value of C mainly influences the transient rate from decay stage to accelerated stage. The final collapse will arrive earlier with the decrease of strength parameter. Besides, we also provide the parametric analysis of the ratio of the upper stress and strength σ_u/C by varying their values in Fig. 5. We can conclude that, keeping a constant ratio σ_u/C , the magnitude of fatigue deformation will increase, although the strength parameter also gets larger with the increase of applied stress.

4.2 Application to Long-Period Cyclic Loads with Constant Upper Limit Stresses

In this subsection, the proposed model will be validated by comparing with mechanical behaviors of salt rock under long-period constant upper limit cyclic loads. The experimental data were reported in Wang et al. (2021). The upper and lower limit stresses of the cyclic load are noted as σ_u and σ_l respectively. The long period of each cycle is noted as T (as shown in Fig. 6). Before predicting the cumulative deformation in cyclic-creep loading, the proposed model is firstly applied to study the instantaneous stage (25) in conventional triaxial compression tests. The elastic parameters of intact materials E and ν , or equivalently k and μ , are determined from the linear parts of stress–strain curves.

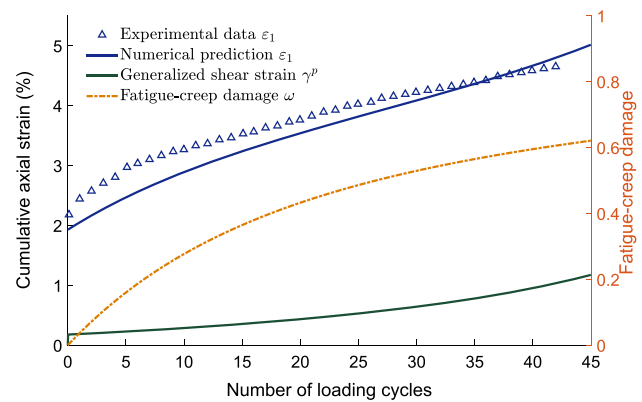
Table 1 Identified values of instantaneous elastoplastic parameters

E (MPa)	ν	A	C (MPa)	α_p^0	B	η
1550	0.21	58	13	0.015	0.0031	-0.0015

**Fig. 8** Evolution of cumulative strain of salt rock subjected to cyclic loading tests under different levels of upper limit stress: comparisons between numerical results (continuous lines) and experimental data (solid symbols reported from Wang et al. 2021)

With the procedure presented above, the values of elastoplastic parameters are given in Table 1. The stress–strain curve in a uniaxial compression test is presented Fig. 7. The numerical results provided by the basic elastoplastic model (25) are compared with the experimental data. A general satisfactory agreement between the numerical and experimental results for axial strain can be observed. The proposed model shows the ability for capturing the main features of short-term mechanical property of tested salt rock, both in the elastic and plastic stages. As a result, the parameters listed in Table 1 will be also adopted in the analysis of cyclic-creep tests.

To simplify the computation for cyclic-creep stage, the damage evolution rate for fatigue and creep is assumed according to the following relation $d\omega_k = (\bar{\omega}_k - \omega_k)(\gamma^f + \gamma^c T^{3.04})dn$ by non-linear fitting. The parameters involved in the description of fatigue damage evolution include γ^f , γ^c , C_1 , and α . They are identified by an optimization procedure by comparing the numerical predictions of cumulative axial strain at peak point of each cycle with the experimental data. Indeed, for this case, the typical three stages of accumulated strain are obtained as that indicated by the green line in Fig. 8 for upper limit stress $\sigma_u = 26$ MPa. This facilitates the determination of all involved parameters. The values obtained for the salt rock in fatigue-creep experiments are as $\gamma^c = 0.000498$, $\gamma^f = 2.5$, $C_1 = 0.76$ and $\alpha = 0.632$. The critical value of generalized plastic strain at peak strength is 0.0271 from the uniaxial compression test. The obtained values are then used for

**Fig. 9** Variations of accumulated axial strain ε_1 , generalized plastic strain γ_p and damage parameter ω for $\sigma_u = 26$ MPa, $T = 4$ h (The experimental data is obtained from Wang et al. 2021)

studying cyclic responses under different upper limit stresses and hold times.

We now firstly present numerical simulations of salt rock under long-period cyclic loads. With the above set of basic mechanical and fatigue-creep damage parameters, the proposed model is used to study the cumulative axial strains in cyclic tests, which were performed under the same lower limit stress ($\sigma_l = 8$ MPa) but 3 different upper limit stresses ($\sigma_u = 18, 22$ and 26 MPa). The period of a single loading-unloading cycle is set as 4 h. So the obtained numerical and experimental cumulative axial strains are plotted in Fig. 8 in different colors. The obtained numerical results are compared with the experimental data for axial strain. Although some simplifications, such as the coupled fatigue-creep damage evolution rate, have been made during the derivation of the model, there is still a good agreement for all levels of upper limit stress. Particularly, depending on the applied upper limit stresses, the proposed model is able to reproduce typical deformation evolution curves. Despite of some small differences at the decay stage, the evolution of total deformation is well described.

For all curves in Fig. 8, an initial instantaneous deformation at the first cycle can always be observed, which is described by the short-term elastoplastic model. But the whole evolution of cumulative axial strain is obviously dependent on the upper limit stress. For lower levels ($\sigma_u = 18$ and 22 MPa), the cumulative axial strain increases rapidly at the decay stage and stabilizes at the steady stage. The value of total cumulative strain is larger when the upper limit stress is higher at the same number of loading cycles. But this is mainly due to the difference on the initial

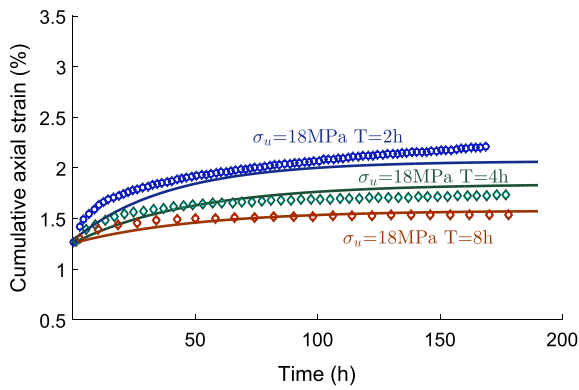


Fig. 10 Evolution of cumulative strain of salt rock subjected to cyclic loading tests with different period of a single cycle: comparisons between numerical results (continuous lines) and experimental data (solid symbols reported from Wang et al. 2021)

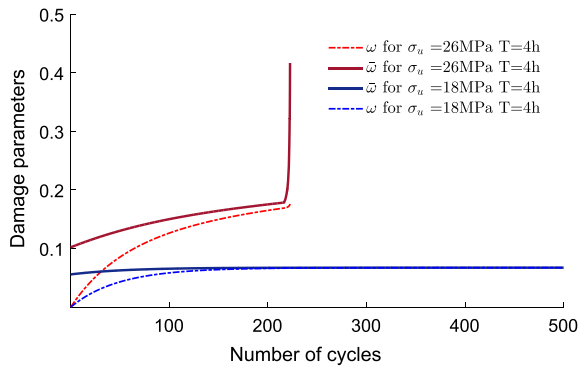
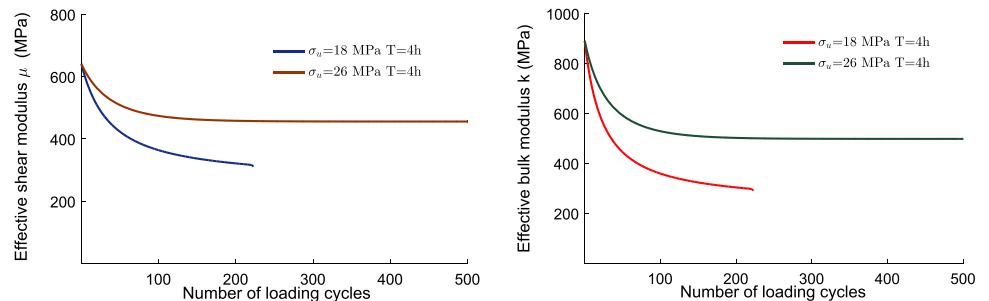


Fig. 11 Evolution of fatigue-creep damage parameter ω and its stationary value $\bar{\omega}$ under different upper limit stresses with a same time period

instantaneous strain. However, it must be pointed out that it does not mean the material remains always in stable state for $\sigma_u = 18$ and 22 MPa. This is due to the accumulation of irreversible plastic strain energy produced in each stabilized cycle (Zhang et al. 2017, 2022), leading eventually to the high-cycle fatigue collapse.

Fig. 12 Evolution of effective shear (left) and bulk (right) moduli during the loading process



On the other hand, for high value of the upper limit stress ($\sigma_u = 26$ MPa), an accelerated evolution phase is produced after the steady stage, as shown in Fig. 8. To better understand the coupling between plastic deformation and fatigue damage, the evolution of generalized plastic strain γ_p and that of fatigue-creep damage parameter ω are plotted in Fig. 9 for the case $\sigma_u = 26$ MPa $T = 4$ h. It is seen that there is a strong correlation between the evolution of axial strain (blue solid line) and that of the damage parameter (orange dash-dot line). The steady stage accounts for the major period of fatigue life. However, the accumulated strain during the steady stage represents only a quite small part of the total quantity, indicating a quasi equilibrium state of the microstructure. Contrarily, the amounts of accumulated strain in the remaining two stages are considerably larger, but the corresponding periods of loading are shorter. According to most fatigue tests, it is generally observed that the upper limit stress and the amplitude of stress variation have a significant influence on the evolution of irreversible cumulative deformation. Besides, the accumulated plastic strain in the cyclic loading process also shows an accelerated trend (see green line in Fig. 9).

For a more detailed analysis of creep effects on accumulated deformation, experimental and numerical results of cumulative strain for 3 different cases of long-period cyclic loads are plotted in Fig. 10. The upper and lower limit stresses are all set as 18 and 8 MPa, respectively. The duration of a single load cycle $T = 2, 4$ and 8 h. The x-axis of Fig. 10 is chosen as holding time for cyclic loads. It is observed that the numerical results are in accordance with experimental data and that the proposed fatigue-creep damage model can describe the creep effects on the long-term deformation. All the strain curves in Fig. 10 start from the same point, since all the upper limit stresses of the cyclic loads are 18 MPa. But the increment rate of the axial strain increases with a smaller value of the time period T . This is due to the fact that more load-unload cycles are carried out on the rock samples for a smaller value of T , leading to more accumulated fatigue-creep damage. The proposed model can capture correctly the material failure by cumulative deformation due to additional fatigue or creep damage.

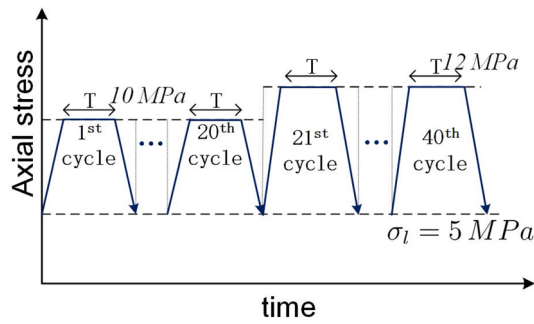


Fig. 13 Schematic diagram of multi-level cyclic loading with constant stress interval

In Fig. 11, we show the evolution of fatigue damage parameter ω and its asymptotic value $\bar{\omega}$ for different upper limit stresses with same period. It should be pointed out that the evolution curve of ω (dash-dot line) for 26 MPa is the same as that plotted in Fig. 9. The corresponding variations of $\bar{\omega}$ are illustrated by the solid lines. It is seen that the stationary condition of fatigue damage, that is $\omega \rightarrow \bar{\omega}$, is progressively approached during the cyclic-creep loading history. The evolution of ω starts from zero value at the first cycle, while the initial value of $\bar{\omega}$ depends on the prescribed upper limit stress. More precisely, for a lower limit stress of $\sigma_u=18$ MPa, the fatigue-creep damage parameter reaches rapidly the value of $\bar{\omega}$ and holds at a stationary value. No failure of material is observed at least within 500 cycles. On the contrary, under a higher limit stress of $\sigma_u=26$ MPa, the fatigue failure occurs due to the rapid increase of $\bar{\omega}$, reflecting the unstable degradation of microstructure.

In Fig. 12, the evolution of effective elastic parameters (bulk and shear moduli) during cyclic-creep loading with the increase of fatigue damage is displayed for two different upper limit stresses. It is clear that the fatigue-creep induced degradation of micro-structure leads to a progressive decrease of elastic modulus. Further, the degradation rate of both bulk and shear moduli is higher for $\sigma_u=26$ MPa than that for $\sigma_u=18$ MPa. In particular, The elastic modulus for $\sigma_u=18$ MPa becomes nearly stationary after the decay stage, while that for $\sigma_u=26$ MPa decreases approximately linearly in the steady stage and falls off a cliff around the fatigue failure, reflecting the different rate of microstructural degradation of material.

Table 2 Identified values of elastic-plastic parameters for multilevel cyclic test

E (MPa)	ν	A_0	C (MPa)	α_p^0	B	η
3400	0.22	51	11	0.0022	0.0011	-0.011

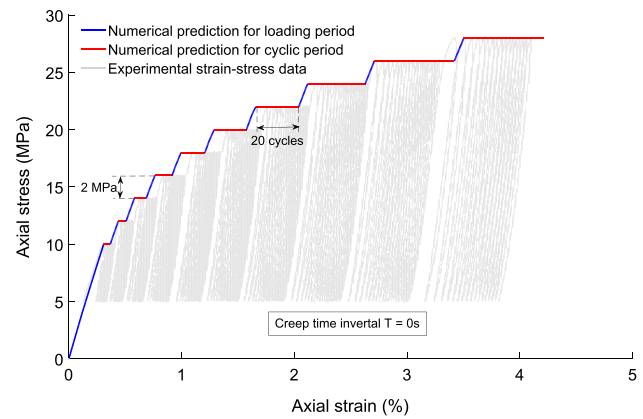


Fig. 14 Comparison of numerical and experimental results (reported from Zhao et al. 2022a) of salt rock under multilevel cyclic loads without stress interval ($T = 0s$)

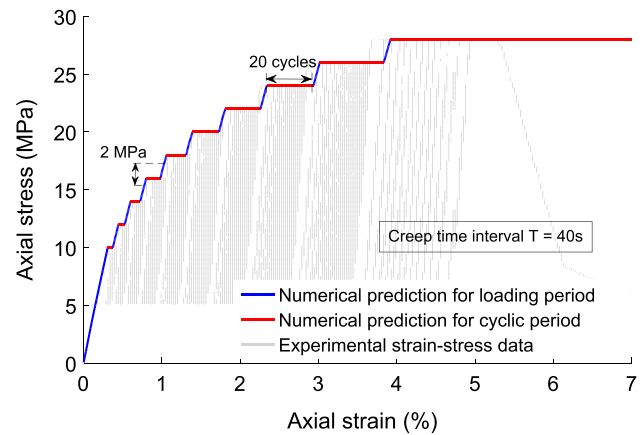
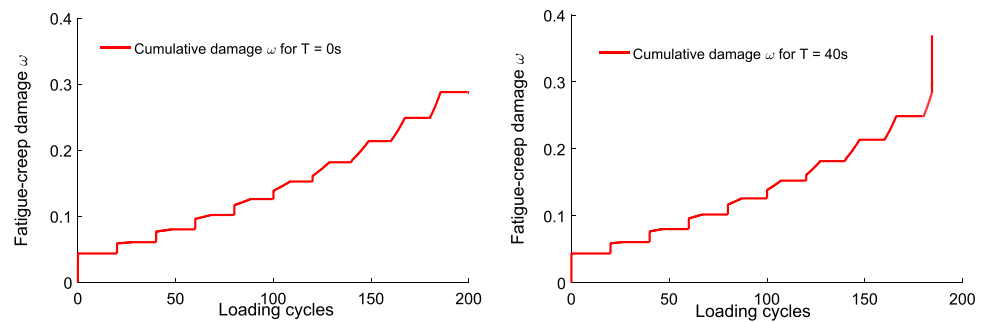


Fig. 15 Comparison of numerical and experimental results (reported from Zhao et al. 2022a) of salt rock under multilevel cyclic loads with constant stress interval ($T = 40s$)

4.3 Application to Multi-level Cyclic Loading with Constant Stress Interval

For further validation of the proposed elastoplastic fatigue-creep damage model, numerical simulations of mechanical responses and damage evolution of salt rock subjected to multi-level cyclic loading with constant stress interval are also carried out. The experimental data are extracted from Zhao et al. (2022a) on Pakistan salt rock. The hold times per cycle T is 0 and 40 s to show the creep effects on the cumulative

Fig. 16 Prediction of cumulative damage in multilevel cyclic loading test with constant stress intervals $T = 0s$ (left) and $T = 40s$ (right)



deformation of salt rock in fatigue-creep tests. Figure 13 presents the loading path, which includes a constant stress interval stage between the loading and unloading phase in a single cycle. The loading path of the multilevel cyclic loading with constant stress intervals consists of two steps: the axial stress was applied to upper limit stress σ_u at stress-controlled mode; the salt sample was subjected to cyclic loading with stress intervals at ten stages. The maximum cyclic stress at the first stage is 10 MPa and increased by 2 MPa for the next stage, and each stage contains 20 cycles. The lower limit stress σ_l is set as 5 MPa for all stages.

By following the same procedure in the previous subsection, the values of elastic-plastic parameters are listed in Table 2. The corresponding fatigue-creep damage values are as $C_1 = 0.31$ and $\alpha = 0.652$. The damage rate parameters are $\gamma^f = 1.66 \times 10^{-4}$ and $\gamma^c = 1.66 \times 10^{-4}$, with the linear relation $d\omega_k = (\bar{\omega}_k - \omega_k)(\gamma^f + \gamma^c T^{-1})dn$ to simplify the computation.

Comparisons between experimental data and numerical predictions by the model have been illustrated in Figs. 14 and 15 without and with constant stress intervals of 40 s, respectively. The pore compaction stage in the first cycle is neglected. The instantaneous mechanical responses in loading period are noted as blue lines and the cumulative strains in cyclic period are in red. In general, a good agreement for both stress loading stage and cyclic stage can be observed. The total deformation throughout the process of multilevel cyclic tests can be easily predicted by the proposed model. Particularly, the stress intervals (Fig. 15) between cycles lead to larger cumulative strains at each stress levels by comparing to those in Fig. 14. Hence, the fatigue fracture occurs in the case of $T = 40s$ at the last stage, while the rock sample does not fail after the cyclic loads without creep effects.

Aiming at presenting the creep effects on the evolution of material degradation, the evolutions of damage parameter for both the above loading cases are plotted in Fig. 16. It is seen that the fatigue-creep damage increases quickly at the first cycle at each stage, and then comes to a steady value for lower stresses. While for higher stresses, the increment rate of damage becomes obviously more important in each cycle. Considering the fatigue-creep condition ($T = 40s$), the damage

parameter is comparatively larger than that without creep load, indicating the additional degradation of microstructure due to creep damage. A sudden jump of damage evolution can also be observed for the last failure cycle. Comparing with the acoustic emission (AE) cumulative energy curves in Zhao et al. (2022a), the evolution of AE energy during the cyclic loading process have a similar trend with that of damage parameter. The AE analysis of salt rock subjected to multilevel cyclic loads are carried out by Zhao et al. (2022a), and briefly presented in Appendix B. Consequently, the property deduction of materials due to microcracks can be predicted, and the acceleration of fatigue damage accumulation due to creep effect is also confirmed by the proposed model.

5 Conclusion

In this study, a novel micromechanical elastoplastic damage model has been established to describe the long-term deformation of quasi-brittle materials subjected to cyclic-creep loading. The degradation of material due to fatigue-creep effect is quantitatively estimated by a micromechanic-based damage variable, by the application of Mori-Tanaka homogenization scheme on the microcracked body. The evolution of fatigue-creep damage is driven by a self-equilibrium state parameter, related to number of loading cycles and hold time. Both the instantaneous and cumulative strain can be predicted by the proposed model in a unified form.

To access the accuracy, the proposed model is numerically implemented in a modified returning mapping procedure. Comparisons between numerical predictions and experimental data for salt rock have been carried out under both constant upper limit cyclic-creep loads and multilevel conditions. A general good agreement is observed for accumulated and plastic strains, and fracture mechanism under different values of upper limit stress with hold time. The damage evolution during loading process is also validated by comparing with the AE energy records. It is found that the creep effect due to hold time of load will lead to an obvious acceleration of fatigue damage accumulation and final fracture of tested material.

Appendix A Micromechanical Damage Parameters α_1 and α_2 of Cracked Material

According to Yuan et al. (2020) and Zhu et al. (2016), the effective elastic tensor C_{ijkl} for heterogeneous materials can be expressed in the general form

$$C_{ijkl}^{\text{eff}} = C_{ijkl} + \sum_{i=1}^N \varphi^{c,i} \left(C_{ijmn}^{c,i} - C_{ijmn} \right) < A_{mnkl} >^{c,i} \quad (1)$$

where C_{ijkl} denotes the initial elastic tensor of solid matrix and $C_{ijmn}^{c,i}$ is that of the i th family of inclusions. $< A_{mnkl} >^{c,i}$ is the mean strain concentration tensor of inclusions in the i th family, and $\varphi^{c,i}$ represents the corresponding volume fraction.

By applying Mori-Tanaka homogenization method, the effective elastic tensor in Eq.(1) can be simplified for open penny-shaped microcracked material as

$$C_{ijkl}^{\text{eff}} = \varphi^0 C_{ijmn} : \left[\varphi^0 I_{mnkl} + \sum_{j=1}^N \varphi^{c,j} \left(I_{mnkl} - S_{mnkl}^c \right)^{-1} \right]^{-1} \quad (2)$$

with φ^0 being the volume fraction for solid phase and Eshelby tensor S_{ijkl}^c is calculated by the use of the fourth-order Hill's tensor P_{mnpq}^c through $S_{ijkl}^c = P_{ijmn}^c C_{mnkl}$.

With the assumption of small volume fraction of microcracks ($\varphi^0 \approx 1$), the effective compliance tensor can be obtained as the inverse of C_{ijkl}^{eff} . Since the cracks are randomly distributed in the solid matrix, the effective compliance tensor is recast into a spherical integration performed over the surface of a unit sphere

$$S_{ijkl}^{\text{eff}} = S_{ijkl} + \frac{\omega}{4\pi} \int_S S_{ijkl}^n dS \quad (3)$$

By applying the surface integration, the effective compliance tensor can be obtained as

$$S_{ijkl}^{\text{eff}} = \frac{1}{3k^{\text{eff}}} J_{ijkl} + \frac{1}{2\mu^{\text{eff}}} K_{ijkl} \quad (4)$$

where the effective bulk and shear moduli of damaged material are

$$k^{\text{eff}} = \frac{1}{1 + \frac{16(1-\nu^2)}{9(1-2\nu)} \omega} k, \quad \mu^{\text{eff}} = \frac{1}{1 + \frac{32(1-\nu)(5-\nu)}{45(2-\nu)} \omega} \mu \quad (5)$$

Comparing with Eq.(5), the micromechanical damage parameters for rock materials containing penny-shaped microcracks take the explicit expressions in (6). It is referred to Yuan et al. (2020) and Zhu et al. (2016) for detailed derivation of micromechanical damage parameters.

Appendix B AE Energy Analysis of Rock Samples Subjected to Multilevel Cyclic Loads with Stress Interval

Multilevel cyclic load tests with constant stress intervals on salt rock were carried out by Zhao et al. (2022a). Damage evolution of the rock material during the loading process were also estimated by the use of acoustic emission (AE) monitoring, related to the initiation and propagation of microcracks. The AE count and energy curves exhibit a similar trend, the evaluations of AE energy during cyclic loading process without and with stress interval are plotted by Zhao et al. (2022a).

It is seen for cyclic load without creep effect, the AE energy presents an active state in the initial deformation stage and a relatively steady value is maintained within one stress level stage. With the increase of stress levels, the accumulation of AE energy during the steady deformation stage generally increases. The growth of the cumulative value of AE energy indicates the degradation degree of salt rock related to the formation and propagation of cracks. On the other hand, the cumulative AE energy increase more rapidly in the initial phase and present a steady increment until the final cycle for the stress interval $T = 40s$. A sudden jump of the AE energy can be observed in the final cycle indicating the rupture of rock sample, which is not seen in the case of $T = 0s$.

The evolution of fatigue-creep damage parameter (Fig. 16) predicted by the proposed model have the similar trends with that observed by AE experiment (Zhao et al. 2022a). Consequently, the degradation of rock material due to fatigue-creep effects can be described by the micromechanical damage model.

Acknowledgements The authors would like to thank the National Natural Science Foundation of China (Grant Nos. 11902111 and 42207226) for the support.

Declarations

competing interests The authors declare that they have no known competing financial interests or personal relationships that could have appeared to influence the work reported in this paper.

References

- Abu-Lebdeh TM, Voyiadjis GZ (1993) Plasticity-damage model for concrete under cyclic multiaxial loading. *J Eng Mech* 119:1465–1484
- Baktheer A, Aguilar M, Chudoba R (2021) Microplane fatigue model ms1 for plain concrete under compression with damage evolution driven by cumulative inelastic shear strain. *Int J Plast* 143:102950
- Carol I, Bazant ZP (1997) Damage and plasticity in microplane theory. *Int J Solids Struct* 34:3807–3835

- Cerfontaine B, Charlier R, Collin F, Taiebat M (2017) Validation of a new elastoplastic constitutive model dedicated to the cyclic behaviour of brittle rock materials. *Rock Mech Rock Eng* 50:2677–2694
- Chiarelli A (2000) Experimental investigation and constitutive modeling of coupled elastoplastic damage in hard claystones. PhD thesis, University of Lille
- Dragon A, Mroz Z (1979) A continuum model for plastic-brittle behaviour of rock and concrete. *Int J Eng Sci* 17:121–137
- Fan J, Chen J, Jiang D, Ren S, Wu J (2016) Fatigue properties of rock salt subjected to interval cyclic pressure. *Int J Fatigue* 90:109–115
- Frantziskonis G, Desai C (1987) Elastoplastic model with damage for strain softening geomaterials. *Acta Mech* 68:151–170
- Ghamgosar M, Erarslan N, Williams D (2017) Experimental investigation of fracture process zone in rocks damaged under cyclic loadings. *Exp Mech* 57:97–113
- He M, Li N, Zhu C, Chen Y, Wu H (2019) Experimental investigation and damage modeling of salt rock subjected to fatigue loading. *Int J Rock Mech Min Sci* 114:17–23
- Jason L, Huerta A, Pijaudier-Cabot G, Ghavamian S (2006) An elastic plastic damage formulation for concrete: Application to elementary tests and comparison with an isotropic damage model. *Comput Methods Appl Mech Eng* 195:7077–7092
- Jia C, Xu W, Wang R, Wang W, Zhang J, Yu J (2018) Characterization of the deformation behavior of fine-grained sandstone by triaxial cyclic loading. *Constr Build Mater* 162:113–123
- Jiang L, Niu D (2016) Study of deterioration of concrete exposed to different types of sulfate solutions under drying-wetting cycles. *Constr Build Mater* 117:88–98
- Jiang R, Dai F, Liu Y, Li A, Feng P (2021) Frequency characteristics of acoustic emissions induced by crack propagation in rock tensile fracture. *Rock Mech Rock Eng* 54:2053–2065
- Kumar SS, Krishna AM, Dey A (2018) Dynamic properties and liquefaction behaviour of cohesive soil in northeast india under staged cyclic loading. *J Rock Mech Geotech Eng* 10:958–967
- Lee J, Fenves GL (1998) Plastic-damage model for cyclic loading of concrete structures. *J Eng Mech* 124:892–900
- Liu X, Ning J, Tan Y, Gu Q (2016) Damage constitutive model based on energy dissipation for intact rock subjected to cyclic loading. *Int J Rock Mech Min Sci* 85:27–32
- Liu Y, Dai F (2018) A damage constitutive model for intermittent jointed rocks under cyclic uniaxial compression. *Int J Rock Mech Min Sci* 103:289–301
- Liu Y, Dai F (2021) A review of experimental and theoretical research on the deformation and failure behavior of rocks subjected to cyclic loading. *J Rock Mech Geotech Eng* 13:1203–1230
- Luccioni BM, Rougier VC (2005) A plastic damage approach for confined concrete. *Comput Struct* 83:2238–2256
- Ma L, Wang Y, Wang M, Xue B, Duan L (2021) Mechanical properties of rock salt under combined creep and fatigue. *Int J Rock Mech Min Sci* 141:104654
- Lj M, Xy L, Wang My X, Hf HR, Px F, Ga W, Qk Y (2013) Experimental investigation of the mechanical properties of rock salt under triaxial cyclic loading. *Int J Rock Mech Mining Sci* 62:34–41
- Miao S, Liu Z, Zhao X, Huang Z (2021) Energy dissipation and damage characteristics of beishan granite under cyclic loading and unloading. *Chin J Rock Mech Eng* 40:928–938
- Moradian Z, Einstein HH, Ballivy G (2016) Detection of cracking levels in brittle rocks by parametric analysis of the acoustic emission signals. *Rock Mech Rock Eng* 49:785–800
- Moreo P, Garcia-Aznar J, Doblare M (2007) A coupled viscoplastic rate-dependent damage model for the simulation of fatigue failure of cement-bone interfaces. *Int J Plast* 23:2058–2084
- Mori T, Tanaka K (1973) Average stress in matrix and average elastic energy of materials with misfitting inclusions. *Acta Metall* 21:571–574
- Pietruszczak S, Jiang J, Mirza F (1988) An elastoplastic constitutive model for concrete. *Int J Solids Struct* 24:705–722
- Pietruszczak S, Lydzba D, Shao JF (2004) Description of creep in inherently anisotropic frictional materials. *J Eng Mech* 130:681–690
- Sandoval C, Malcher L, Canut F, Araújo L, Doca T, Araújo J (2020) Micromechanical gurson-based continuum damage under the context of fretting fatigue: influence of the plastic strain field. *Int J Plast* 125:235–264
- Shao JF, Jia Y, Kondo D, Chiarelli AS (2006) A coupled elastoplastic damage model for semi-brittle materials and extension to unsaturated conditions. *Mech Mater* 38:218–232
- Shao JF, Zhu QZ, Su K (2003) Modeling of creep in rock materials in terms of material degradation. *Comput Geotech* 30:549–555
- Shi Z, Li J, Wang J (2022) Effect of creep load on fatigue behavior and acoustic emission characteristics of sandstone containing pre-existing crack during fatigue loading. *Theoret Appl Fract Mech* 119:103296
- Singh A, Kumar C, Kannan LG, Rao KS, Ayothiraman R (2018) Estimation of creep parameters of rock salt from uniaxial compression tests. *Int J Rock Mech Min Sci* 107:243–248
- Sun Q, Zhang Y (2019) Combined effects of salt, cyclic wetting and drying cycles on the physical and mechanical properties of sandstone. *Eng Geol* 248:70–79
- Tang JH, Chen XD, Dai F (2020) Experimental study on the crack propagation and acoustic emission characteristics of notched rock beams under post-peak cyclic loading. *Eng Fract Mech* 226:106890
- Vaneghi RG, Ferdosi B, Okoth AD, Kuek B (2018) Strength degradation of sandstone and granodiorite under uniaxial cyclic loading. *J Rock Mech Geotech Eng* 10:117–126
- Wang J, Li J, Shi Z (2022) Deformation damage and acoustic emission characteristics of red sandstone under fatigue-creep interaction. *Theoret Appl Fract Mech* 117:103192
- Wang J, Zhang Q, Song Z, Zhang Y (2021) Experimental study on creep properties of salt rock under long-period cyclic loading. *Int J Fatigue* 143:106009
- Wang Y, Ma L, Fan P, Chen Y (2016) A fatigue damage model for rock salt considering the effects of loading frequency and amplitude. *Int J Min Sci Technol* 26:955–958
- Wang Z, Li S, Qiao L, Zhao J (2013) Fatigue behavior of granite subjected to cyclic loading under triaxial compression condition. *Rock Mech Rock Eng* 46:1603–1615
- Wu JY, Li J, Faria R (2006) An energy release rate-based plastic-damage model for concrete. *Int J Solids Struct* 43:583–612
- Xiao JQ, Feng XT, Ding DX, Jiang FL (2011) Investigation and modeling on fatigue damage evolution of rock as a function of logarithmic cycle. *Int J Numer Anal Meth Geomech* 35:1127–1140
- Yang SQ, Ranjith P, Huang YH, Yin PF, Jing HW, Gui YL, Yu QL (2015) Experimental investigation on mechanical damage characteristics of sandstone under triaxial cyclic loading. *Geophys J Int* 201:662–682
- Yang SQ, Tian WL, Ranjith P (2017) Experimental investigation on deformation failure characteristics of crystalline marble under triaxial cyclic loading. *Rock Mech Rock Eng* 50:2871–2889
- Ye D, Wang Z (2001) A new approach to low-cycle fatigue damage based on exhaustion of static toughness and dissipation of cyclic plastic strain energy during fatigue. *Int J Fatigue* 23:679–687
- Yuan S, Zhu Q, Zhao L, Chen L, Zhang J (2020) Micromechanical modelling of short- and long-term behavior of saturated quasi-brittle rocks. *Mech Mater* 142:2
- Zhang J, Shao J, Zhu Q, De Saxcé G (2022) A bipotential-based macroscopic fatigue criterion of porous materials with a pressure-sensitive and non-associated plastic solid matrix and comparison with numerical simulation. *Mech Mater* 165:104161

- Zhang J, Shen W, Oueslati A, De Saxcé G (2017) Shakedown of porous materials. *Int J Plast* 95:123–141
- Zhang Y, Chen Y, Yu R, Hu L, Irfan M (2017) Effect of loading rate on the felicity effect of three rock types. *Rock Mech Rock Eng* 50:1673–1681
- Zhao K, Ma H, Liang X, Li X, Liu Y, Cai R, Ye L, Yang C (2022) Damage evaluation of rock salt under multilevel cyclic loading with constant stress intervals using ae monitoring and ct scanning. *J Petrol Sci Eng* 208:109517
- Zhao K, Ma H, Zhou J, Yin H, Li P, Zhao A, Shi X, Yang C (2022) Rock salt under cyclic loading with high-stress intervals. *Rock Mech Rock Eng* 2:1–19
- Zhao L, Zhu Q, Xu W, Dai F, Shao JF (2016) A unified micromechanics-based damage model for instantaneous and time-dependent behaviors of brittle rocks. *Int J Rock Mech Min Sci* 84:187–196
- Zhou Y, Sheng Q, Li N, Fu X, Zhang Z, Gao L (2020) A constitutive model for rock materials subjected to triaxial cyclic compression. *Mech Mater* 144:103341
- Zhu Q, Zhao L, Shao J (2016) Analytical and numerical analysis of frictional damage in quasi brittle materials. *J Mech Phys Solids* 92:137–163
- Zhu Q, Zhou C, Shao JF, Kondo D (2010) A discrete thermodynamic approach for anisotropic plastic-damage modeling of cohesive-frictional geomaterials. *Int J Numer Anal Meth Geomech* 34:1250–1270
- Zhu QZ, Kondo D, Shao J (2008) Micromechanical analysis of coupling between anisotropic damage and friction in quasi brittle materials: role of the homogenization scheme. *Int J Solids Struct* 45:1385–1405
- Zhu QZ, Zhao LY, Liu HX, Shao JF (2016) Fast explicit integral algorithms with comparative studies for shao-zhu-su rock rheological model. *Chin J Rock Mech Eng* 35(02):242–249

Publisher's Note Springer Nature remains neutral with regard to jurisdictional claims in published maps and institutional affiliations.

Springer Nature or its licensor (e.g. a society or other partner) holds exclusive rights to this article under a publishing agreement with the author(s) or other rightsholder(s); author self-archiving of the accepted manuscript version of this article is solely governed by the terms of such publishing agreement and applicable law.